OPEN

Experimental & Molecular Medicine (2017) 49, e377; doi:10.1038/emm.2017.135
Official journal of the Korean Society for Biochemistry and Molecular Biology
www.nature.com/emm

ORIGINAL ARTICLE

Follistatin N terminus differentially regulates muscle size and fat *in vivo*

Hui Zheng[1,2,3], Chunping Qiao[1,3], Ruhang Tang[1], Jianbin Li[1], Karen Bulaklak[1], Zhenhua Huang[1], Chunxia Zhao[1], Yi Dai[1], Juan Li[1] and Xiao Xiao[1]

Delivery of follistatin (FST) represents a promising strategy for both muscular dystrophies and diabetes, as FST is a robust antagonist of myostatin and activin, which are critical regulators of skeletal muscle and adipose tissues. FST is a multi-domain protein, and deciphering the function of different domains will facilitate novel designs for FST-based therapy. Our study aims to investigate the role of the N-terminal domain (ND) of FST in regulating muscle and fat mass *in vivo*. Different FST constructs were created and packaged into the adeno-associated viral vector (AAV). Overexpression of wild-type FST in normal mice greatly increased muscle mass while decreasing fat accumulation, whereas overexpression of an N terminus mutant or N terminus-deleted FST had no effect on muscle mass but moderately decreased fat mass. In contrast, FST-I-I containing the complete N terminus and double domain I without domain II and III had no effect on fat but increased skeletal muscle mass. The effects of different constructs on differentiated C2C12 myotubes were consistent with the *in vivo* finding. We hypothesized that ND was critical for myostatin blockade, mediating the increase in muscle mass, and was less pivotal for activin binding, which accounts for the decrease in the fat tissue. An *in vitro* TGF-beta1-responsive reporter assay revealed that FST-I-I and N terminus-mutated or -deleted FST showed differential responses to blockade of activin and myostatin. Our study provided direct *in vivo* evidence for a role of the ND of FST, shedding light on future potential molecular designs for FST-based gene therapy.
Experimental & Molecular Medicine (2017) **49,** e377; doi:10.1038/emm.2017.135; published online 15 September 2017

INTRODUCTION

Myostatin, also known as growth/differentiation factor-8 (GDF8), is a member of the transforming growth factor β (TGF-β) superfamily. Myostatin acts as a negative regulator of muscle development.[1–5] The biological function of myostatin has raised the possibility of using its inhibitors to promote muscle growth and improve disease phenotypes in a variety of primary and secondary myopathies, including muscular dystrophies.[6–11] Myostatin inhibitors include the myostatin propeptide,[1] follistatin (FST)[12] and the FST-related gene (FLRG),[13] as well as growth and differentiation factor-associated serum protein-1 (GASP-1).[14] Among them, FST is the most potent inhibitor.

Activin is another member of the TGF-β superfamily and binds to FST with high affinity.[15,16] It is involved in a variety of physiological functions, including metabolism, immunity and reproduction.[17–20] Activin B is involved in energy expenditure, whereas Activin A has a critical role in proliferation and differentiation of human adipose progenitor cells.[20,21] The significant increase in activin A, which may lead to insulin resistance and inflammation, is more often observed in obese subjects than lean ones.[21,22] In addition, our recent study indicates that overexpression of FST in the pancreas of the type 2 diabetic mouse ameliorates disease symptoms by promoting β-cell proliferation via bioneutralization of activin A and myostatin.[23] Therefore, blocking activin A and myostatin through delivery of FST in diabetic patients could represent a new therapeutic avenue.

FST, first recognized as a follicle-stimulating hormone (FSH) inhibitor, is an autocrine glycoprotein that is expressed in nearly all tissues of higher animals.[24,25] Its primary function is binding and bioneutralization of members of the TGF-β superfamily, particularly activins, followed by myostatin (growth/differentiation factor-8, GDF8), GDF9, and BMPs 2, 5, 7 and 8.[26,27]

FST is synthesized in three protein isoforms: FST-288, FST-303 and FST-315.[16,28,29] FST-315 is the predominant form accounting for 95% of all FSTs.[25] It consists of the N-terminal

[1]Division of Pharmacoengineering and Molecular Pharmaceutics, Eshelman School of Pharmacy, University of North Carolina, Chapel Hill, NC, USA and [2]Department of Neurology, Nanfang Hospital, Southern Medical University, Guangdong, People's Republic of China
[3]These authors contributed equally to this work.
Correspondence: Dr X Xiao, Division of Pharmacoengineering and Molecular Pharmaceutics, Eshelman School of Pharmacy, University of North Carolina, 120 Mason Farm Road, CB# 2070, 2077 Genetic Medicine Building, Chapel Hill, NC 27599, USA.
E-mail: xxiao@email.unc.edu
Received 13 December 2016; revised 10 February 2017; accepted 8 March 2017

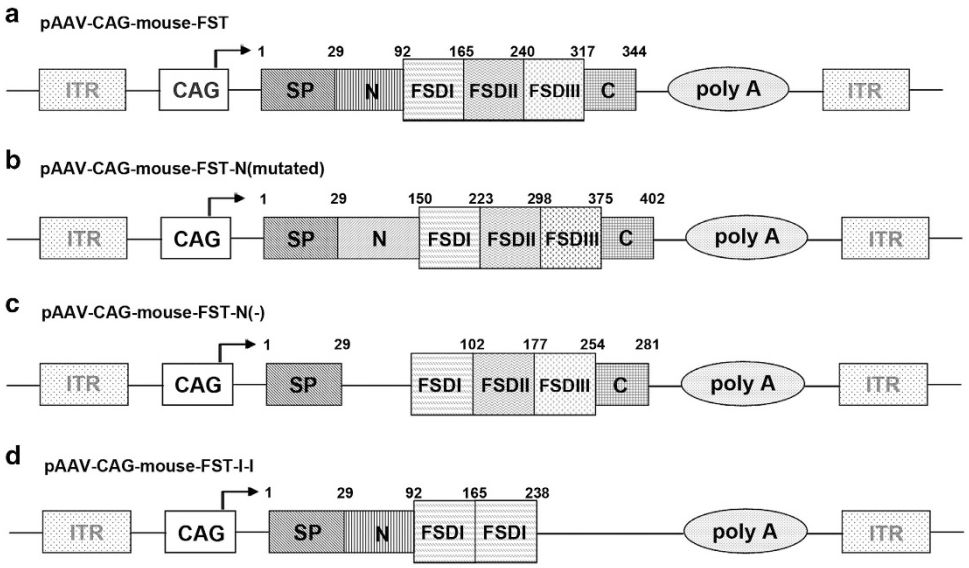

Figure 1 FST vector constructs. (**a**) Mouse FST cDNA. (**b**) FST-N-mutated plasmid containing a mutated N terminus. (**c**) FST-N(−) plasmid containing deleted N terminus. (**d**) FST-I-I plasmid containing two copies of domain I with a complete N terminus SP, signal peptide; ITR, inverted terminal repeats; CAG, a hybrid promoter contains the cytomegalovirus enhancer, chicken beta-actin promoter and rabbit beta-globin intron. N, N-terminal; FSD I, FST domain I; FSD II, FST domain II; FSD III, FST domain III; C, C terminus.

domain (ND), three follistatin domains (FSD1, FSD2 and FSD3) and a C-terminal tail containing several acidic residues, which decrease its heparin binding affinity.[25,30] FST-315 is found primarily in blood circulation. FST-288 lacks the C-terminal tail and is a tissue bound isoform, whereas FST-303 contains only part of the C-terminal tail and is gonad-specific.[31]

It is widely accepted that FSD1 and FSD2 significantly contribute to binding affinity, but findings concerning the importance of the ND and whether it is necessary for activin and myostatin binding are mixed.[32–36] Structural and biochemical evidence have suggested that deletion or truncation of the ND or disruption of N-terminal disulfides each reduced activin binding to $<5\%$ of the expressed wild-type (WT) FST or abolished it.[27,37,38] However, previous studies of the FST crystal structure have indicated that the ND had important roles in myostatin binding but not in activin binding.[36] An FST construct consisting of the complete ND followed by two FSD1s was reported to exhibit high affinity for myostatin binding, but not activin binding.[39] This indicates that different domains of FST differentially regulate FST-myostatin and FST-activin interactions. Given the controversial function of ND of FST in binding with myostatin and activin, this study aims to investigate the ND of FST via an *in vivo* mouse study.

MATERIALS AND METHODS

Construction of FST plasmids and AAV vector production

The mouse FST cDNA (GenBank accession number: NM_008046) was generated by reverse transcription polymerase chain reaction (PCR) method from the ovary tissues of normal female ICR mice, and the primers used were 5′-CAG GAT GGT CTG CGC CAG-3′ and 5′-GTT TTG CCC AAA GGC TAT GTC-3′. The PCR product was initially cloned into the EcoRV site of pBluescript-KS(+) (BSKS) backbone. Then, the *Sac*I–*Xho*I fragment of pBSKS-FST was cloned into an AAV vector plasmid via sticky end ligation. The mouse-FS-N (mutated) sequence (30–92 amino acids of the N terminus of wild-type FST were replaced with the 29–150 amino acids of GenBank XM_005619457) was directly synthesized by the GenScript company (Piscataway, NJ 08854). The FS-N(−) (30–92 amino acids of the N terminus were deleted) and FST-I-I (containing the complete N terminus and double domain I without domain II and III) were generated by site-directed mutagenesis based upon the pBSKS-FST template. The various FST genes were cloned into the same AAV vector plasmid (pXX-CAG) under the transcriptional control of the chicken β-actin (CAG) promoter including cytomegalovirus (CMV) enhancers and a large synthetic intron (Figure 1).[40]

Recombinant viral vector stocks were produced according to the plasmid co-transfection method.[41] Viral particles were purified twice by CsCl density gradient ultracentrifugation using a previously published protocol.[42] Vector titers were determined by the DNA dot-blot method and were in the range of 2×10^{12} to 5×10^{12} vector genomes (vg) per ml.

Mice and vector administration

All experiments involving animals were approved by the University of North Carolina Animal Care and Use Committee and the male ICR mice were purchased from Taconic. All the vectors were delivered into 4-week-old ICR mice (18–22 g) by tail vein injection. AAV9-CAG-mouse-FST was delivered at a final dose of 2.5×10^{11} vg per mouse, and other viruses were injected at 5×10^{11} vg per mouse. Control mice were injected with PBS. Body weight of the mice was measured once a week starting from 2 weeks after injection until the mice were 12 weeks old.

Muscle and fat morphology, morphometric analysis and immunofluorescence staining

TA (tibialis anterior), GAS (gastrocnemius) and other muscles were collected at the indicated age, and H&E (hematoxylin and eosin) staining was performed on 9-μm frozen sections using a previously reported method.[7] The abdominal white fat tissue was separated from other tissues after opening the abdominal wall of the mice. Total

abdominal white fat from each mouse was weighed and H&E staining was performed on 5-μm paraffin embedded sections.

For morphometric analysis, thin cryosections of TA and GAS muscles from treated and control mice (four mice per group) were subjected to a rabbit polyclonal antibody recognizing human dystrophin rod 22 and rod 23 region (diluted 1:500, generated in Dr Xiao's lab) staining for displaying the periphery of the muscle fibers.[43] Pictures were taken, and the total area of each myofiber was analyzed with MetaMorph software (Molecular Devices, Sunnyvale, CA, USA). The average myofiber size (from at least 150 myofibers per mouse) was calculated and used for the statistical analysis.

For immunofluorescent staining, frozen sections were permeabilized with permeabilization buffer (1% Triton X-100 in PBS) for 15 min at room temperature. After blocking with 10% horse serum (HS) in PBS, the sections were incubated with rabbit anti-phosphorylated-Smad2/3 antibody (1:500, Santa Cruz Biotechnology INC, Cat# sc-11769R) overnight. The ratios of phosphorylated-Smad2/3 positive muscle fibers to total muscle fibers were calculated from 40× images. All TA and GAS muscles were imaged and total muscle fiber numbers were counted by counting DAPI (4′,6-diamidine-2′-phenylindole dihydrochloride)-stained nuclei. For each mouse, approximately 500 muscle fibers of TA and 1000 of GAS were counted.

Western blotting

Protein of the TA muscle (or differentiated C2C12 cells) was extracted using lysis buffer containing 1% Triton X-100, 20 mM Tris-HCL (pH 7.5), 150 mM NaCl, 1 mM EDTA, 5 mM NaF, 2.5 mM sodium pyrophosphate, 1 mM beta-glycerophosphate, 1 mM Na_3VO_4, 1 μg ml^{-1} leupeptin, 0.1 mM PMSF and a cocktail of protease inhibitors (Sigma, St Louis, MO, USA, Cat# P0044). 25 μg of protein per lane and prestained molecular weight markers (Bio-Rad, Hercules, CA, USA Cat# 161–0318) were separated with 12% SDS/PAGE gels and then transferred to polyvinylidene fluoride (PVDF) membranes. After blocking at room temperature for 1 h with a solution containing 3% bovine serum albumin (BSA, Fisher Scientific, Waltham, MA, USA, Cat# 137043) in 10 mM Tris-HCl (pH 7.5), 100 mM NaCl and 0.1% Tween-20 (TBST), membranes were incubated overnight at 4 °C with 1:500 rabbit polyclonal anti-phosphorylated-AKT (Ser473) (Cell Signaling, Danvers, MA, USA, Cat# 9271), rabbit anti-phosphorylated-Smad2/3 antibody (1:1000), or GAPDH (1:5000, Sigma, Cat# G9545), followed by 1:5000 horseradish peroxidase (HRP)-conjugated secondary antibody incubation. A chemiluminescent detection kit (PerkinElmer, Waltham, MA, USA, Cat# 203–100901) was used to develop the membranes.

Culture and treatment of C2C12 cell line

The conditioned media was produced by transfection of individual plasmid into the 293 cells using the calcium phosphate method. Seven to 12 h after transfection, the media was replaced by Opti-Mem media (Gibco, Life Technologies, Carlsbad, CA USA. REF # 31985-070). The supernatant of the transfected 293 cells was collected 48–60 h after transfection as the conditioned media.

C2C12 cells were cultured in growth medium consisting of Dulbecco's modified Eagle's medium (DMEM, Gibco, Life Technologies, Cat# 1676966), supplemented with 10% Fetal Bovine Serum (FBS, HyClone, GE Healthcare Life Sciences, Logan, UT, USA) and 1/3 conditioned media. Differentiation was initiated 24 h after seeding by changing to conditioned differentiation medium, consisting of DMEM, supplemented with 2% HS and 1/3 conditioned media. The conditioned differentiation medium was renewed every 2–3 days until C2C12 cells were fully differentiated.

To analyze changes in myotube size, differentiated myotubes were fixed with ice-cold acetone and methanol (1:1) for 10 min at 4°. After washing with PBS three times, cells were permeabilized with 1% Triton X-100 in PBS for 10 min, blocked with 10% horse serum for 1 h, then subjected to dystrophin R22R23 antibody staining for displaying peripheral edges.

The diameter of the myotubes was measured using Adobe Photoshop software (Adobe, Los Altos, CA, USA). The width of each myotube was measured three times in different spots and the average reading was obtained. For each group, a minimum of 50 myofibers were measured.

Luciferase reporter assays

The 293-cell line was utilized in an activin blockade assay; 293 cells were plated onto 6-well plates at $\sim 2 \times 10^5$ cells per well 1 day before transfection. For all wells, the TGF-beta1-responsive luciferase reporter p3TP-Lux (0.1 μg per well) and transfection control CMV-LacZ plasmids (0.1 μg per well) were transfected using the calcium phosphate method. In addition, distinct plasmids (2.8 μg per well) such as pBluescript-KS(+), pAAV-CAG-mouse-FST, pAAV-CAG-mouse-N(−), pAAV-CAG-mouse-N(mutated) or pAAV-CAG-mouse-FST-I-I were transfected into each well, respectively. Six to eight hours after transfection, the transfection media were replaced either by activin-conditioned media (DMEM supplemented with 2% FBS and 1/3 activin-conditioned media) or Bluescript-KS(+)-conditioned media. The transfected cells were collected 36 h after transfection. Luciferase activities were measured with a luciferase assay kit (Promega, Cat# E1501), and LacZ activity was measured using the classic colorimetric ONPG assay method.[44] The luciferase activities were normalized by LacZ activity.

For the myostatin blockade experiment, the R-1B L17 cells were used.[45] The R-1B L17 cells were plated onto 6-well plates at $\sim 2.5 \times 10^5$ cells per well 1 day before transfection. Transfection was performed with Lipofectamine 3000 transfection kit (Invitrogen, Life Technologies, Carlsbad, CA, USA, Cat# 1662152). For all the wells, the 3TP-Lux plasmid (0.2 μg per well), transfection control CMV-LacZ plasmids (0.1 μg per well) and pCMV5b-ALK4 plasmids (1.1 μg per well) were transfected. In addition, different induction and control plasmids (1.1 μg per well) were added. Six to eight hours after transfection, the transfection media were replaced either by myostatin-conditioned media or Bluescript-KS(+)-conditioned media. The transfected cells were harvested and luciferase activities were examined as described above.

Statistical analysis

Values are expressed as the mean ± s.e.m. All statistical analyses were performed in GraphPad Prism software using a one- or two-way analysis of variance (ANOVA) with a Dunnett post-test. $P < 0.05$ was considered statistically significant.

RESULTS

Delivery of N(−) or N-mutant FST in adult mice failed to increase skeletal muscle mass

We constructed AAV vectors containing intact, N terminus-mutated and -deleted FST genes. In addition, we created an FST-I-I construct comprised of the full N terminus, double domain I and C terminus without domains II and III. It has been reported that the FST domain I (FSD1) is responsible for the myostatin inhibition effect, and the FST-I-I construct (Figure 1d) retains myostatin binding with weaker activin

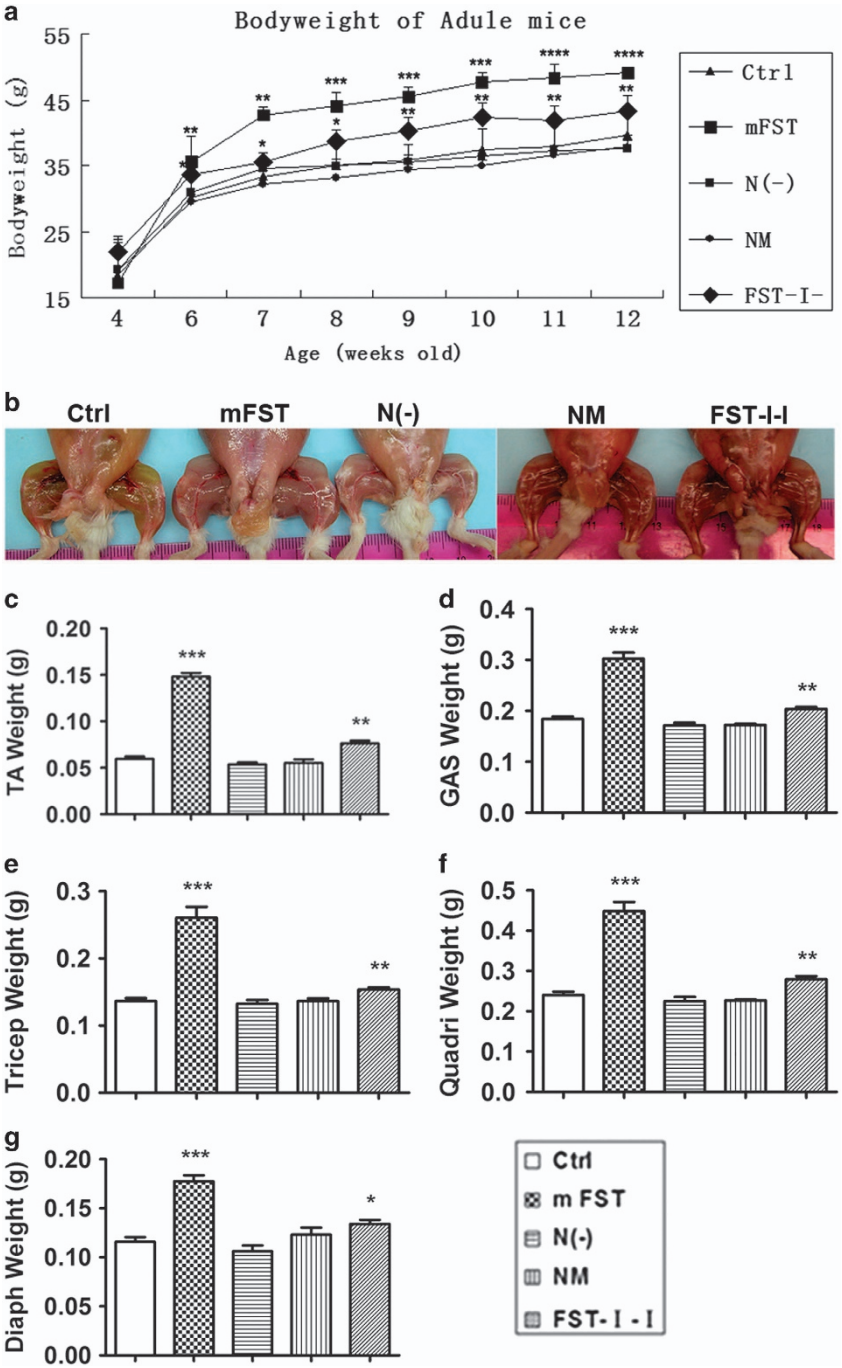

Figure 2 Delivery of N(−) or NM to adult mice failed to increase skeletal muscle mass. (**a**) Body weight of the AAV9-CAG-mouse-FST group (large square) was significantly increased compared with the control group from 6 weeks old (2 weeks after injection), while that of the AAV9-CAG-mouse-FST-I-I group (diamond) was slightly increased. There was no difference in mouse weight in the AAV9-CAG-mouse-N(−) (small square) group and AAV9-CAG-mouse-FST-NM (asterisk) group compared with the control group (triangle). (**b**) Images of hind leg muscles of different groups. Compared with the control group, muscles of the FST-I-I group were slightly larger and muscles of the FST group were the largest. There was no difference among N(−), NM and control groups. (**c**–**g**) Muscle weights of different groups. TA muscle weight (**c**), GAS muscle weight (**d**), the triceps muscle weight (**e**), the quadriceps muscle weight (**f**) and the diaphragm muscle weight (**g**) increased in FST and FST-I-I young adult mice group, whereas those of N(−) and NM did not. $N=4$ for all groups unless otherwise specified. $^{*}P<0.05$, $^{**}P<0.01$, $^{***}P<0.001$ and $^{****}P<0.0001$ compared with control ICR mice.

blockade activity.[33,35] The FST genes were driven by ubiquitous CAG promoter (see the 'Materials and Methods' section for details), and the plasmids were named pAAV-CAG-mouse-FST (Figure 1a), pAAV-CAG-mouse-FST-NM (mutated) (Figure 1b), pAAV-CAG-mouse-FST-N(−) (Figure 1c) and pAAV-CAG-FST-I-I (Figure 1d), respectively. The expression of FST-based plasmids was revealed via western blot (Supplementary Figure 1).

The four different AAV constructs were packaged into the AAV9 vector, which has been shown to have a superior ability to transduce cardiac muscle, skeletal muscle and liver cells via systemic delivery.[46,47] The AAV9 vectors containing varied FST genes were injected into 4-week-old adult mice by the tail vein ($2.5–5 \times 10^{11}$ vg per mice). The control group was injected with saline PBS. After vector administration, the mice were periodically weighed to determine whether their weight was affected by the treatment. As shown in Figure 2a, compared with the body weight of saline-treated control mice (30.2 g), we observed a significant weight increase in the AAV9-CAG-mouse-FST group (FST, 35.6 g, $P=0.006$), an intermediate weight increase in the AAV9-CAG-mouse-Follistatin-I-I group (FST-I-I, 33.7 g, $P=0.035$), and no weight increase for AAV9-CAG-mouse-Follistatin-N(−) (N(−), 30.9 g, $P=0.33$) and AAV9-CAG-mouse-Follistatin-N(mutated) (NM, 29.6 g, $P=0.38$) groups, starting from 2 weeks after vector injection (6-week-old). The mice were euthanized 8 weeks after vector delivery (12-week-old). Different muscle groups were carefully dissected and weighed (Figure 2b). There was an obvious increase in weight of major skeletal muscles after FST and FST-I-I vector delivery, but no difference was found among control, NM and N(−) groups (Figure 2c–g).

Cryosections were made from various muscle groups and H&E staining was performed to examine muscle fiber size (Figure 3a). The expression of different FST constructs was confirmed by immunofluorescent staining (Supplementary Figure 2a) and western blot (Supplementary Figure 2b). Similar to the results obtained from whole body and muscle weights, obvious hypertrophy was found in the FST group (tibialis anterior (TA) muscle: 2.17-fold over control, $P<0.001$; gastrocnemius (GAS) muscle: 2.8-fold over control, $P<0.001$). A minor increase was observed in the FST-I-I muscles (TA: 1.1-fold over control, $P>0.05$; GAS: 1.4-fold over control, $P<0.05$) (Figure 3b). The muscles from N(−) and N (mutated) groups displayed normal histology without changes in myofiber size compared with those of untreated control mice (Figure 3a and b). Because an increase in skeletal muscle mass is a hallmark of myostatin inhibition, we conclude from these data that the FST with an N terminus mutation or deletion has lost its apparent myostatin blockade effect *in vivo*.

Involvement of signaling pathways in skeletal muscles by FST-based constructs

To understand the molecular mechanisms of the FST constructs in skeletal muscles, IF staining and western blot were performed to detect the relevant signaling pathways, particularly the inhibition of Smad2/3 and the activation of insulin-phosphoinositide 3-kinase (PI3K)-AKT pathways. The level of intra-nuclear phosphorylated Smad2/3 (P-Smad) of the TA muscle was examined by IF staining (Figure 3c). The percentage of P-Smad2/3^{+} nuclei/total nuclei in the FST group was significantly inhibited compared with the control mice ($17.7 \pm 6.4\%$ vs $96.2 \pm 3.5\%$, $n=3$, $P<0.0001$), followed by the FST-I-I group ($43.8 \pm 3.9\%$ vs $96.2 \pm 3.5\%$, $P<0.0001$) (Figure 3d). Surprisingly, we also noticed inhibition of P-Smad2/3 levels in both FST-N (mutated) ($53.2 \pm 2.6\%$, $P<0.001$) and N(−) ($59.1 \pm 6.2\%$, $P<0.001$) groups compared with the controls, albeit to a lesser extent (Figure 3d).

The PI3K–AKT pathway can also impact muscle fiber size.[48,49] To explore the role of this pathway in skeletal muscles after injection of different FST-based constructs, western blot was performed against phosphorylated AKT (P-AKT) (Figure 3e). Both FST (2.1 ± 0.2-fold greater than the control for the ratio of P-AKT/total AKT, $n=3$, $P<0.01$) and FST-I-I groups (2.1 ± 0.2-fold greater than the control, $n=3$, $P<0.05$) showed significant activation of P-AKT. There was only a marginal increase in P-AKT expression in both N(−) (1.2 ± 0.02-fold greater than the control, $n=3$, $P>0.05$) and NM (1.6 ± 0.1-fold greater than the control, $n=3$, $P>0.05$) groups (Figure 3f). Our results indicated weak ligand binding abilities and inefficient intracellular signaling mediated by both N(−) and NM constructs in skeletal muscles.

FST-N(−) or FST-NM in adult mice partially decreased white adipose tissue mass

The weight of white adipose tissue (WAT) from different anatomical sites was evaluated during the tissue harvest (Figure 4a). As expected, a significant decrease in WAT weight was observed in the FST group ($24.3 \pm 11.8\%$ of the control, $P<0.001$). In addition, we noticed a decrease in WAT weight for both N(−) ($48.8 \pm 14.4\%$ of the control, $P<0.01$) and NM ($57.1 \pm 26.5\%$ of the control, $P<0.05$) groups (Figure 4b). However, there was no significant difference in WAT weight in the FST-I-I group ($98.0 \pm 31.8\%$ of the control, $P>0.05$) compared with the control (Figure 4b).

To examine individual adipocyte sizes, cryosections were made and H&E staining was performed. Consistent with the WAT weight data, we observed a significant decrease in adipocyte sizes in the FST group. N(−) and NM groups also displayed smaller adipocyte sizes, whereas the FST-I-I group did not change in size compared with the control (Figure 4c). From these data, we concluded that FST with an N terminus mutation or deletion were able to decrease white fat *in vivo*.

N terminus-mutated or -deleted FSTs minimally enhanced differentiation of C2C12 myoblasts

To evaluate the *in vitro* effects of different FST constructs on differentiation of myofibers, we investigated them on C2C12 myoblasts. The C2C12 cells were cultured in differentiation media supplemented with conditioned media collected from 293 cells transfected with different constructs (GFP control, mouse-FST, mouse-FST-N (mutated), mouse-N(−) and mouse-FST-I-I). After 4 days of differentiation, the FST group appeared much larger than the control GFP group, followed by the FST-I-I, NM and N(−) groups (Figure 5a). Quantitation data showed that the myofiber diameter of the FST group (666.5 ± 271.2 μm, $n=156$, $P<0.001$) were 2.05-fold larger than the control myotubes (323.5 ± 106.5 μm, $n=729$), and the FST-I-I group (596.0 ± 217.2 μm, $n=199$, $P<0.01$) were 1.8-fold larger (Figure 5b). The NM group (482.2 ± 160.5 μm, $n=217$, $P<0.05$) and N(−) group (414.9 ± 161.7 μm, $n=187$,

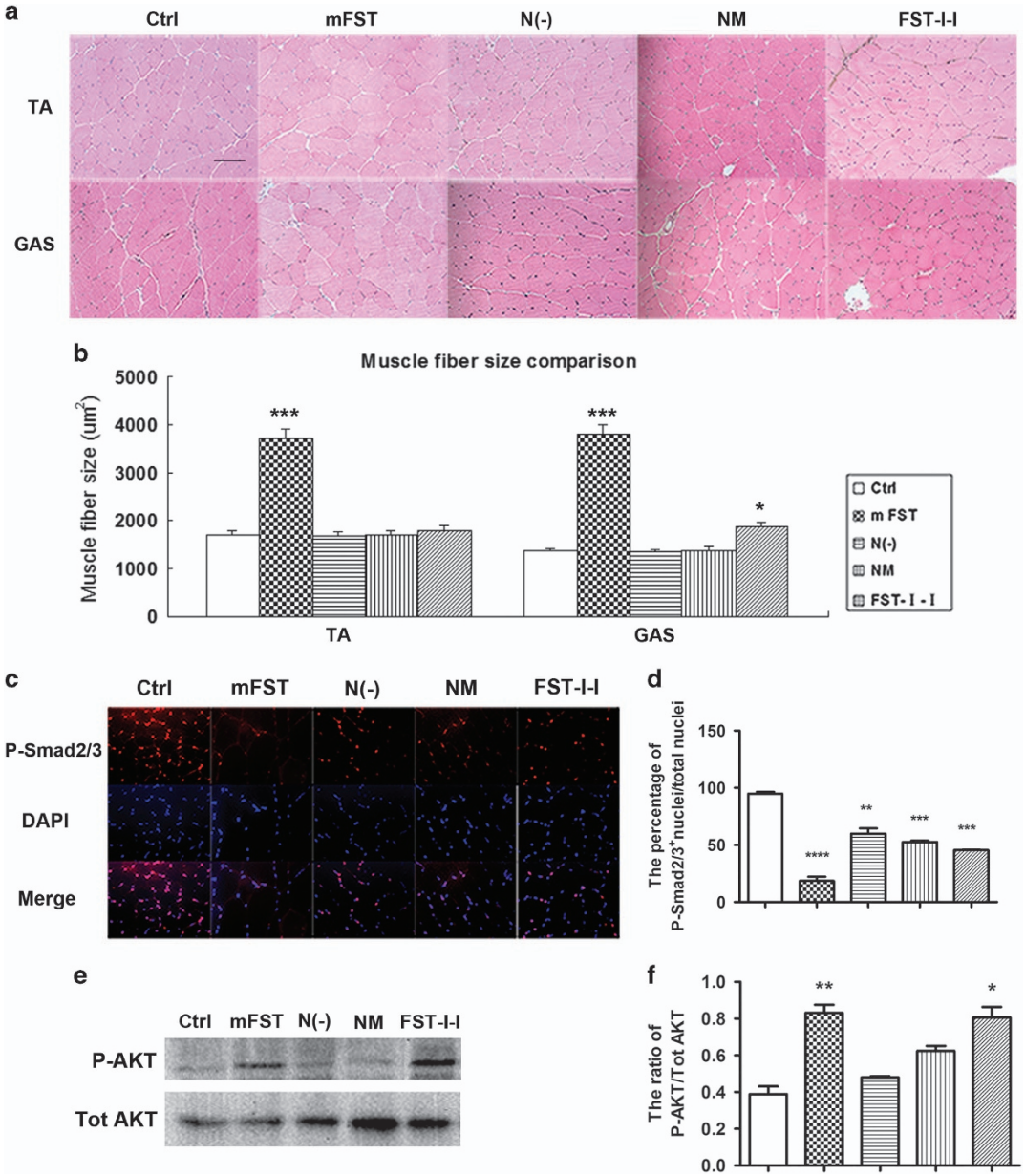

Figure 3 Delivery of N(−) or NM to adult mice failed to increase myofiber sizes in adult mice and had minimal involvement in relevant signaling pathways. (**a**) H&E staining of TA and GAS muscles (20×). Scale bar: 100 μm. (**b**) Quantification of muscle fiber size. TA and GAS fiber size of FST were 2.2- and 2.8-fold over the control, respectively. Those of the FST-I-I muscles were 1.1- and 1.4-fold greater than the control. However, N(−) and NM muscles displayed normal histology without changes in myofiber size or number compared with those of untreated control mice. $*P<0.05$, $**P<0.01$, $***P<0.001$ and $****P<0.0001$ compared with control ICR mice. (**c**) Immunofluorescent staining of muscle fibers against P-Smad2/3. Red indicates P-Smad2/3-positive cells, and blue indicates the nucleus (DAPI-stained). (**d**) Quantification of the percentage of phospho-SMAD2/3 nuclear positive cells to total muscle fibers. In the FST group, the percentage was significantly decreased compared with the control group (17.7 ±6.4% vs 96.2 ± 3.5%), whereas the percentage of FST-I-I was 43.8 ± 3.9%, N(−) was 59.1 ±6.2% and NM was 53.2 ± 2.6%. (**e**) The expression of phosphorylated AKT (P-AKT, ser 473) and total AKT (Tot AKT) was shown by western blot. (**f**) Semi-quantification of P-AKT expression shown in the western blot. Compared with the control group, the expression of P-AKT to total AKT in FST was 2.1-fold greater, FST-I-I was 2.1-fold greater, N(−) was 1.2-fold greater and NM was 1.6-fold greater. $*P<0.05$, $**P<0.01$, $***P<0.001$ and $****P<0.0001$ compared with control ICR mice. $N=4$ for all groups.

$P>0.05$) showed minimal enhancement by 1.5-fold and 1.3-fold, respectively (Figure 5b).

It has been reported that myostatin binds to its receptor complex ActRIIB/ALK4 or ALK5 on the skeletal muscle, resulting in both activation of Smad2/3 and inhibition of the PI3K intracellular signaling pathways. The alteration of these two pathways impacts protein synthesis, which ultimately causes muscle atrophy.[48,49] To understand the molecular

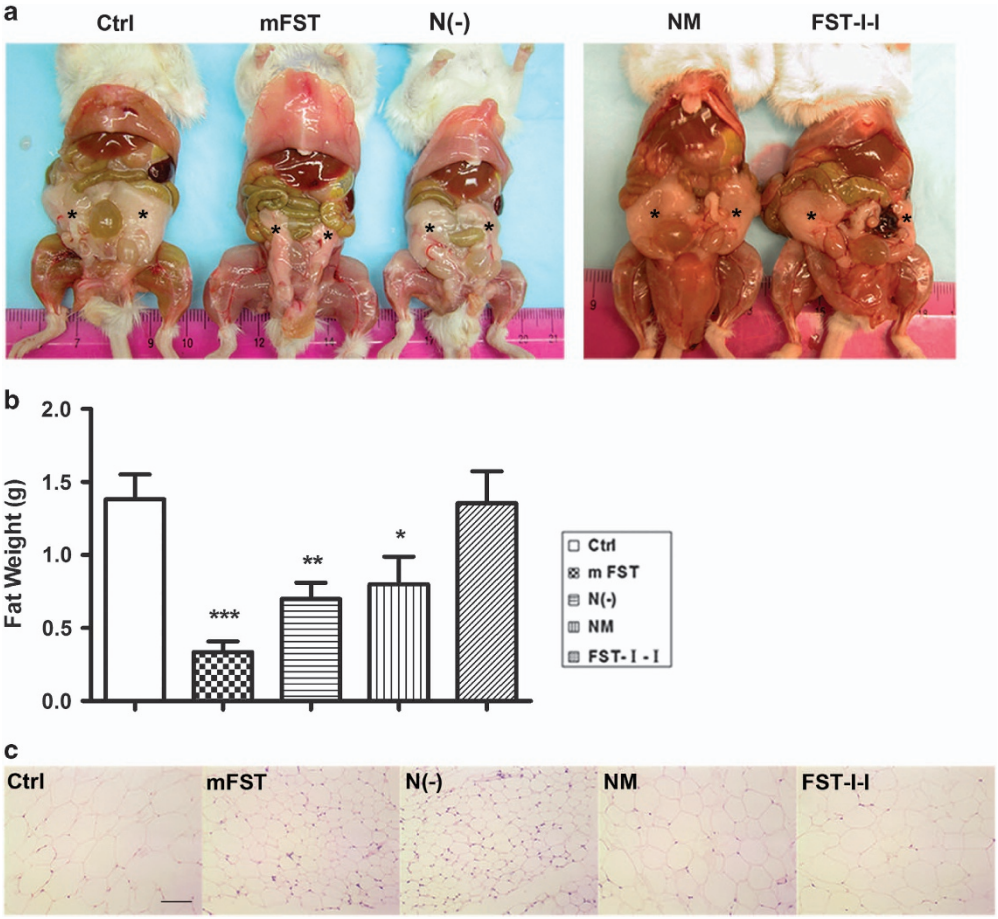

Figure 4 Delivery of N(−) or NM to adult mice decreased white adipose tissue mass. (**a**) Images of abdominal fat (stars) among treatment groups. (**b**) Quantification of the abdominal fat. An obvious decrease in WAT mass was found after FST vector delivery (24.3% of the control). Although not as obvious as FST, the WAT mass of N(−) (48.8% of the control) and NM were significantly decreased (57.1% of the control). The WAT mass of the FST-I-I group did not change compared with the control (98% of the control). (**c**) The H&E staining of white adipose tissue (20×), scale bar: 100 μm. $N=5$, $^{*}P<0.05$, $^{**}P<0.01$ and *** $P<0.001$ compared with the control ICR mice.

mechanisms in myotube diameter change caused by different FST-based constructs, we performed a western blot against P-Smad2/3 vs total Smad and P-AKT vs total AKT in C2C12 cells with different culture conditions. Western blots showed that Smad2/3 was significantly inhibited in the FST group (74.4% of the control for the ratio of P-Smad2/3/total Smad, $P<0.01$), followed by the FST-I-I group (84.2% of the control, $P<0.05$) (Figure 6a and b). NM and N(−) had no apparent influence on the expression of P-Smad2/3. In contrast, all the constructs significantly upregulated AKT signaling in the differentiated C2C12 cells, with the FST being the highest (369.6% of the ratio of P-AKT/total AKT of control, $P<0.0001$), followed by FST-I-I (310.4% of the control for the ratio of P-AKT/total AKT, $P<0.0001$), N(−) (282.8% of control, $P<0.001$) and FST-N (mutated) (162.8% of the control, $P<0.001$) (Figure 6c and d). These results indicate that both blockade of Smad and activation of the AKT pathways could contribute to enlargement of the differentiated myotubes, and the N(−) and NM constructs had minimal effects on Smad signaling in cultured myotubes *in vitro*.

The effect of FST-based constructs on SMAD luciferase reporter assay

Our data indicated that N(−) and NM significantly decreased white fat weight with a minimal impact on muscle mass. Because it is well known that FST can markedly increase muscle mass in normal mice through blockade of myostatin,[1–5] we reasoned that decreased fat mediated by FST was mainly through activin. We hypothesized that ND was critical for myostatin blockade, but less pivotal for activin interaction. To test this hypothesis, we utilized a luciferase reporter gene with the 3TP promoter that contains three consecutive TPA (tetradecanoylphorbol-13-acetate) responsive elements and one TGF-β responsive element (p3TP-Lux, Addgene, Cambridge, MA, USA, Cat# 11767).[50] This reporter system is often used to test the transcriptional activity of TGF-β signaling.[51–55]

In the myostatin blockade reporter assay, four plasmids were co-transfected into R-1B (L17) cells, a mink lung epithelial cell line expressing very low amounts of TGF-β superfamily type I receptor. These four plasmids include 3TP-Lux, a transfection control plasmid (CMV-LacZ), ALK4 (activin receptor-like kinase-4, a type I receptor) expression plasmid and various

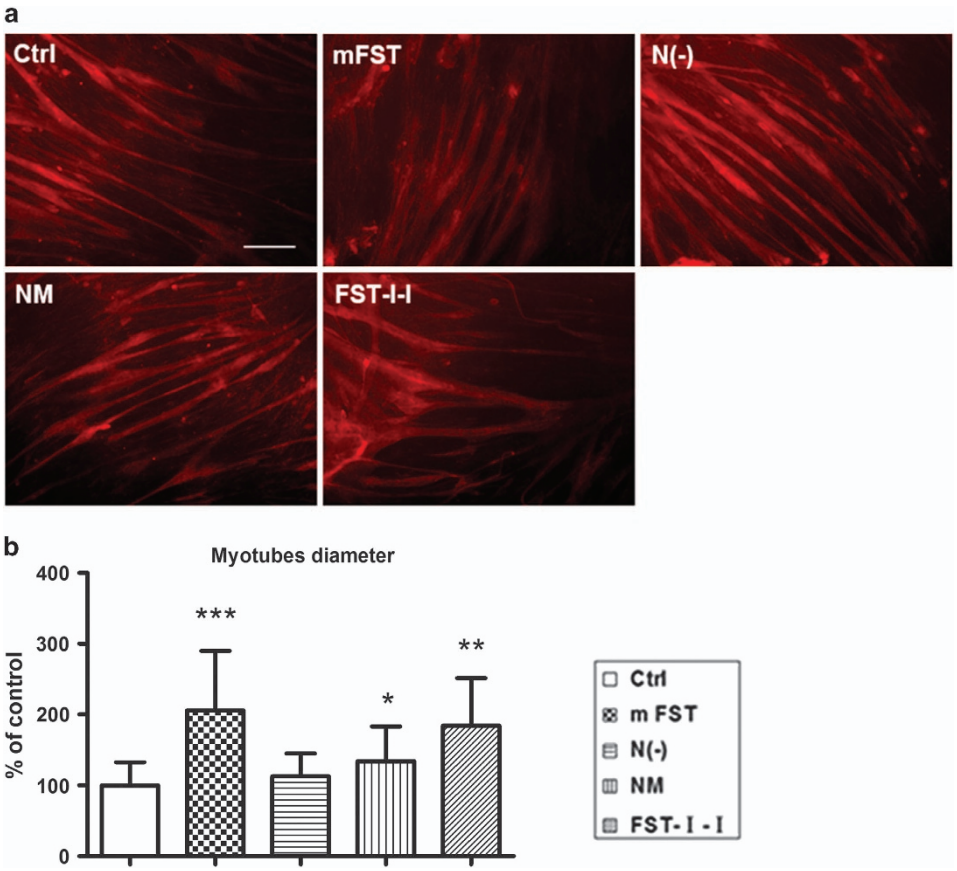

Figure 5 N terminus-mutated or -deleted FSTs had minimal effect on the differentiation of C2C12 myoblasts. (**a**) Immunofluorescent staining of differentiated C2C12 myoblasts against dystrophin. The C2C12 cells were cultured under differentiation media supplemented with conditioned media containing control (GFP) plasmid, mouse-FST, mouse-NM, mouse-N(−) and mouse-FST-I-I plasmids as indicated in the figure. We found that C2C12 cells cultured with all FST vectors were larger in diameter than the control. FST and FST-I-I-conditioned media showed the greatest increase, whereas NM and N(−) groups were only slightly larger. Scale bar: 100 μm. (**b**) The measurement of diameters of differentiated C2C12 myotubes. Myotubes cultured with mouse-FST-conditioned media were 2.1-fold larger, whereas FST-I-I was 1.8-fold larger, N(−) was 1.3-fold larger and NM was 1.5-fold larger than the control. $^{*}P<0.05$, $^{**}P<0.01$ and $^{***}P<0.001$ compared with control ICR mice.

FST-based constructs (see the 'Materials and Methods' section for details). Myostatin was supplied in the culture media 8 h after transfection as conditioned media. As expected, FST significantly decreased luciferase expression induced by myostatin (27.9% of the control, $P<0.0001$, Figure 7a). FST-I-I also significantly inhibited myostatin, albeit to a lesser degree (45.6% of the control, $P<0.01$). N(−) (51.4% of control, $P<0.05$) and NM (56.5% of control, $P>0.05$) demonstrated the least myostatin inhibition.

For the activin neutralization assay, we utilized 293 cells. Therefore, the myostatin receptor ALK4 plasmid was not needed. Three plasmids (3TP-Lux, cmv-LacZ and varied FST-based constructs) were co-transfected into the 293 cells. Activin was provided in the culture media 8 h after transfection as conditioned media (see materials and methods for details). As expected, FST significantly inhibited the luciferase expression elicited by activin (27.6% of control, $P<0.01$), whereas N(−)(48.8% of control, $P<0.05$) and NM (39.6% of control, $P<0.05$) also substantially blocked the luciferase expression. The FST-I-I construct containing the complete N terminus displayed minimal activin neutralization effects (74.4% of control, $P>0.05$) (Figure 7b). The results of our luciferase reporter assay fully support our hypothesis that the N terminus of FST is more important for myostatin binding than activin bioneutralization.

DISCUSSION

FST is recognized as an important regulator of cell secretion, development and differentiation in a number of tissues and organ systems. FST functions through its ability to potently bind and antagonize TGF-β superfamily ligands. TGF-β superfamily ligands signal by binding to specific cell receptors (two type II and two type I), which in turn activate the canonical SMAD-mediated pathway and non-SMAD pathways.[36] In addition, the diverse functions of TGF-β superfamily ligands arise through its regulation at multiple levels, beginning at the ligands, the receptors and at the level of transcription activation complex formation.[56] FST was first identified as a potent inhibitor of activin but is now known to bind other ligands, including inhibin; bone morphogenetic proteins (BMPs) 2, 4, 6, 7, 11 and

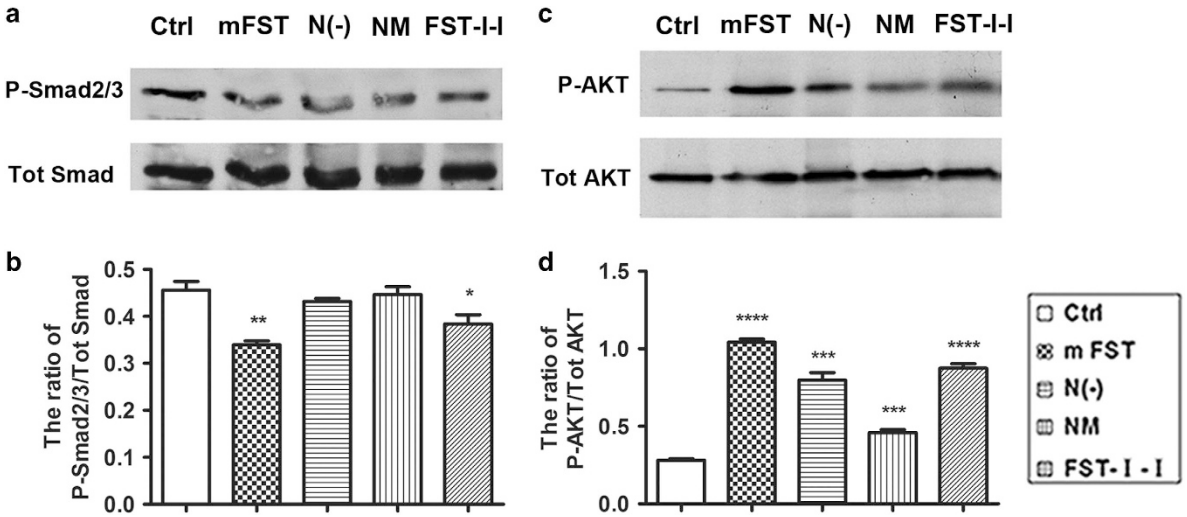

Figure 6 Minimal involvement of relevant signaling pathways by N terminus-mutated or -deleted FSTs in differentiated C2C12 myoblasts. (**a**) Western blot against P-Smad2/3 and total SMADs in differentiated C2C12 myoblasts. (**b**) Semi-quantification of pSmad expression shown in the western blot as the ratio of P-Smad2/3 to total Smads. Compared with the control, the ratio of P-Smad2/3 to total Smads was downregulated by FST to 74.4% and FST-I-I to 84.2%, indicating the Smad pathway inhibition, whereas N(−) and NM groups did not change much (the ratio was 94.7% and 97.9%, respectively). (**c**) Western blot against P-AKT and total AKT in differentiated myoblast. (**d**) Semi-quantification of pAKT expression. The ratio of P-AKT to total AKT was greatly activated by FST followed by FST-I-I, N(−) and NM. $*P<0.05$, $**P<0.01$, $***P<0.001$ and $****P<0.0001$ compared with control.

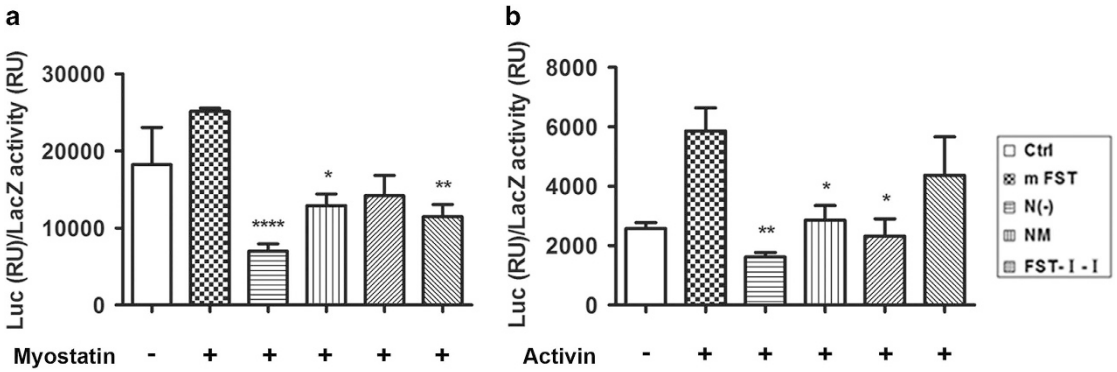

Figure 7 The effect of various FST-based constructs on the Smad luciferase reporter assay. (**a**) The myostatin blockade reporter assay. The L17R-1B cells were utilized here, and myostatin was provided as the conditioned media. FST and FST-I-I significantly inhibited the luciferase expression induced by myostatin to 27.9% and 45.6% of the control, respectively. NM (56.5%) or N(−) (51.4%) had milder blockade effects against myostatin. (**b**) Activin blockade reporter assay. The 293 cells were used here, and the activin was supplied as the conditioned media. FST significantly decreased luciferase expression induced by activin to 27.6% of the control, followed by N(−)(48.8% of the control) and NM (39.6% of the control). FST-I-I (74.4% of the control) had no significant activin inhibitory effects. $*P<0.05$, $**P<0.01$, $***P<0.001$ and $****P<0.0001$ compared with control.

15; and myostatin, with lower affinities.[57–59] Numerous *in vitro* structural and biochemical studies have predicted the function of different domains of FST.[36,37,60] For example, by studying crystal structure, Cash *et al.*[36] reported that the N-terminal domain of FST undergoes conformational rearrangements to bind myostatin and likely acts as a site of specificity for the antagonist. Utilizing an *in vitro* bioassay system, Sidis *et al.*[37] demonstrated that the N-terminal domain of FST had an essential role in activin binding and neutralization. To our knowledge, this was the first study to provide direct *in vivo* evidence reflecting the importance of the N-terminal of FST in regulating biological effects of myostatin and activin.

The most important finding of our study was that N(−) or NM constructs did not increase muscle weight, yet decreased white fat mass *in vivo*. It is well known that FST can significantly increase skeletal muscle weight *in vivo* partly through blockade of myostatin.[12,61] Our data imply that ND is critical for myostatin binding, and therefore, the N terminus-deleted or -mutated FST constructs failed to increase muscle mass. This further validates the importance of ND in the interaction of FST with myostatin by blocking type I receptor binding sites as revealed by crystal structure.[36] In contrast, the FST-I-I construct with the complete N terminus and lacking domain II and domain III increased skeletal muscle mass while leaving the white fat weight unchanged. Our data are in agreement with other studies indicating that transgenic expression of the FST-I-I construct increases skeletal muscle mass.[35] However, the FST-I-I transgenic mice also displayed decreased fat accumulation, which is different

from our finding that fat weight was unchanged.[34] We believe the discrepancy is due to the degree of myostatin inhibition in fat tissue. Transgenic technology would result in stronger myostatin inhibition than gene transfer, which was used in our study. Further investigation involving higher vector dosage and earlier intervention (such as neonatal treatment) with the same vector should resolve the discrepancy. Nevertheless, our data suggest the essential role that ND had in blockade of myostatin.

There is a debate as to how critical the ND is to the interaction of FST with activin. In one instance, deletion or mutation of the N-terminal domain of FST prevented activin binding and failed to suppress the bioactivity of activin *in vitro*.[37] Other studies indicate that FST domains I and II are the major contributors to FST-activin interactions.[62,63] In the present study, we performed an *in vivo* experiment revealing that both N(−) and NM could significantly decrease white fat mass. The mechanism by which FST decreases white fat tissue is complicated given that numerous FST binding ligands are involved in adipocyte development, adiposity and energy expenditure.[64] Considering both N(−) and NM had limited ability to block myostatin, we hypothesized that the fat decreasing effect observed in those two groups were mainly through binding with activin, which possesses a strong binding affinity to FST. Our *in vitro* Smad reporter assay revealed that both constructs could inhibit luciferase activity induced by activin, indicating both could bind with activin. Therefore, our study indicates that the N-terminal domain of FST is not critical for binding activin.

In summary, TGF-β superfamily members and their related signal transduction pathways have gained great attention in adipogenesis, mature adipocyte function, pancreatic β-cell proliferation, as well as muscle pathogenesis in recent years. Blockade of the TGF-β transduction pathway through FST is an emerging therapeutic avenue for treating diabetes and muscular dystrophies. Our results will provide further evidence for rational designs of FST-based therapies.

CONFLICT OF INTEREST

The authors declare no conflict of interest.

ACKNOWLEDGEMENTS

This work was supported by NIH grants R01 NS079568 and R01 NS082536 awarded to XX and Project 81100938-H0911 from the National Natural Science Foundation of China awarded to HZ.
We thank Dr Quan Jin for critical reading of the manuscript.

Author contributions: HZ, CQ and XX designed the study and wrote the paper. HZ performed and analyzed all experiments. CQ helped analyze the experiments shown in Figures 2,4 and 7. JBL helped to make AAV viruses for this project. RT performed and analyzed the experiments shown in Figure 6. YD provided technical assistance. JL supervised the study. All authors reviewed the results and approved the final version of the manuscript.

1 Lee SJ, McPherron AC. Regulation of myostatin activity and muscle growth. *Proc Natl Acad Sci USA* 2001; **98**: 9306–9311.
2 McPherron AC, Lawler AM, Lee SJ. Regulation of skeletal muscle mass in mice by a new TGF-beta superfamily member. *Nature* 1997; **387**: 83–90.
3 Yang J, Ratovitski T, Brady JP, Solomon MB, Wells KD, Wall RJ. Expression of myostatin pro domain results in muscular transgenic mice. *Mol Reprod Dev* 2001; **60**: 351–361.
4 Zhu X, Hadhazy M, Wehling M, Tidball JG, McNally EM. Dominant negative myostatin produces hypertrophy without hyperplasia in muscle. *FEBS Lett* 2000; **474**: 71–75.
5 Whittemore LA, Song K, Li X, Aghajanian J, Davies M, Girgenrath S *et al.* Inhibition of myostatin in adult mice increases skeletal muscle mass and strength. *Biochem Biophys Res Commun* 2003; **300**: 965–971.
6 Tsuchida K. Targeting myostatin for therapies against muscle-wasting disorders. *Curr Opin Drug Discov Dev* 2008; **11**: 487–494.
7 Qiao C, Li J, Jiang J, Zhu X, Wang B, Li J *et al.* Myostatin propeptide gene delivery by adeno-associated virus serotype 8 vectors enhances muscle growth and ameliorates dystrophic phenotypes in mdx mice. *Hum Gene Ther* 2008; **19**: 241–254.
8 Qiao C, Li J, Zheng H, Bogan J, Li J, Yuan Z *et al.* Hydrodynamic limb vein injection of adeno-associated virus serotype 8 vector carrying canine myostatin propeptide gene into normal dogs enhances muscle growth. *Hum Gene Ther* 2009; **20**: 1–10.
9 Benabdallah BF, Bouchentouf M, Tremblay JP. Improved success of myoblast transplantation in mdx mice by blocking the myostatin signal. *Transplantation* 2005; **79**: 1696–1702.
10 Benabdallah BF, Bouchentouf M, Rousseau J, Bigey P, Michaud A, Chapdelaine P *et al.* Inhibiting myostatin with follistatin improves the success of myoblast transplantation in dystrophic mice. *Cell Transplant* 2008; **17**: 337–350.
11 Fakhfakh R, Michaud A, Tremblay JP. Blocking the myostatin signal with a dominant negative receptor improves the success of human myoblast transplantation in dystrophic mice. *Mol Ther* 2001; **19**: 204–210.
12 Rodino-Klapac LR, Haidet AM, Kota J, Handy C, Kaspar BK, Mendell JR. Inhibition of myostatin with emphasis on follistatin as a therapy for muscle disease. *Muscle Nerve* 2009; **39**: 283–296.
13 Hill JJ, Davies MV, Pearson AA, Wang JH, Hewick RM, Wolfman NM *et al.* The myostatin propeptide and the follistatin-related gene are inhibitory binding proteins of myostatin in normal serum. *J Biol Chem* 2002; **277**: 40735–40741.
14 Hill JJ, Qiu Y, Hewick RM, Wolfman NM. Regulation of myostatin in vivo by growth and differentiation factor-associated serum protein-1: a novel protein with protease inhibitor and follistatin domains. *Mol Endocrinol* 2003; **17**: 1144–1154.
15 Nakamura T, Takio K, Eto Y, Shibai H, Titani K, Sugino H. Activin-binding protein from rat ovary is follistatin. *Science* 1990; **247**: 836–838.
16 Sidis Y, Mukherjee A, Keutmann H, Delbaere A, Sadatsuki M, Schneyer A. Biological activity of follistatin isoforms and follistatin-like-3 is dependent on differential cell surface binding and specificity for activin, myostatin, and bone morphogenetic proteins. *Endocrinology* 2006; **147**: 3586–3597.
17 Mayer K, Buchbinder A, Morty RE. Activin A: a mediator governing inflammation, immunity, and repair. *Am J Respir Crit Care Med* 2012; **185**: 350–352.
18 Muttukrishna S, Tannetta D, Groome N, Sargent I. Activin and follistatin in female reproduction. *Mol Cell Endocrinol* 2004; **225**: 45–56.
19 Hashimoto O, Funaba M. Activin in glucose metabolism. *Vitam Horm* 2011; **85**: 217–234.
20 Li L, Shen JJ, Bournat JC, Huang L, Chattopadhyay A, Li Z *et al.* Activin signaling: effects on body composition and mitochondrial energy metabolism. *Endocrinology* 2009; **150**: 3521–3529.
21 Zaragosi LE, Wdziekonski B, Villageois P, Keophiphath M, Maumus M, Tchkonia T *et al.* Activin a plays a critical role in proliferation and differentiation of human adipose progenitors. *Diabetes* 2010; **59**: 2513–2521.
22 Dani C. Activins in adipogenesis and obesity. *Int J Obes* 2013; **37**: 163–166.
23 Zhao C, Qiao C, Tang RH, Jiang J, Li J, Martin CB *et al.* Overcoming insulin insufficiency by forced follistatin expression in beta-cells of db/db mice. *Mol Ther* 2015; **23**: 866–874.
24 Patel K. Follistatin. *Int J Biochem Cell Biol* 1998; **30**: 1087–1093.
25 Phillips DJ, de Kretser DM. Follistatin: a multifunctional regulatory protein. *Front Neuroendocrinol* 1998; **19**: 287–322.
26 Amthor H, Nicholas G, McKinnell I, Kemp CF, Sharma M, Kambadur R *et al.* Follistatin complexes Myostatin and antagonises Myostatin-mediated inhibition of myogenesis. *Dev Biol* 2004; **270**: 19–30.
27 Thompson TB, Lerch TF, Cook RW, Woodruff TK, Jardetzky TS. The structure of the follistatin:activin complex reveals antagonism of both type I and type II receptor binding. *Dev Cell* 2005; **9**: 535–543.

28 Saito S, Sidis Y, Mukherjee A, Xia Y, Schneyer A. Differential biosynthesis and intracellular transport of follistatin isoforms and follistatin-like-3. *Endocrinology* 2005; **146**: 5052–5062.
29 Schneyer AL, Wang Q, Sidis Y, Sluss PM. Differential distribution of follistatin isoforms: application of a new FS315-specific immunoassay. *J Clin Endocrinol Metab* 2004; **89**: 5067–5075.
30 Hashimoto O, Kawasaki N, Tsuchida K, Shimasaki S, Hayakawa T, Sugino H. Difference between follistatin isoforms in the inhibition of activin signalling: activin neutralizing activity of follistatin isoforms is dependent on their affinity for activin. *Cell Signal* 2000; **12**: 565–571.
31 Sugino K, Kurosawa N, Nakamura T, Takio K, Shimasaki S, Ling N *et al.* Molecular heterogeneity of follistatin, an activin-binding protein. Higher affinity of the carboxyl-terminal truncated forms for heparan sulfate proteoglycans on the ovarian granulosa cell. *J Biol Chem* 1993; **268**: 15579–15587.
32 Harrison CA, Chan KL, Robertson DM. Activin-A binds follistatin and type II receptors through overlapping binding sites: generation of mutants with isolated binding activities. *Endocrinology* 2006; **147**: 2744–2753.
33 Schneyer AL, Sidis Y, Gulati A, Sun JL, Keutmann H, Krasney PA. Differential antagonism of activin, myostatin and growth and differentiation factor 11 by wild-type and mutant follistatin. *Endocrinology* 2008; **149**: 4589–4595.
34 Nakatani M, Kokubo M, Ohsawa Y, Sunada Y, Tsuchida K. Follistatin-derived peptide expression in muscle decreases adipose tissue mass and prevents hepatic steatosis. *Am J Physiol Endocrinol Metab* 2011; **300**: E543–E553.
35 Nakatani M, Takehara Y, Sugino H, Matsumoto M, Hashimoto O, Hasegawa Y *et al.* Transgenic expression of a myostatin inhibitor derived from follistatin increases skeletal muscle mass and ameliorates dystrophic pathology in mdx mice. *FASEB J* 2008; **22**: 477–487.
36 Cash JN, Rejon CA, McPherron AC, Bernard DJ, Thompson TB. The structure of myostatin:follistatin 288: insights into receptor utilization and heparin binding. *EMBO J* 2009; **28**: 2662–2676.
37 Sidis Y, Schneyer AL, Sluss PM, Johnson LN, Keutmann HT. Follistatin: essential role for the N-terminal domain in activin binding and neutralization. *J Biol Chem* 2001; **276**: 17718–17726.
38 Stamler R, Keutmann HT, Sidis Y, Kattamuri C, Schneyer A, Thompson TB. The structure of FSTL3.activin A complex. Differential binding of N-terminal domains influences follistatin-type antagonist specificity. *J Biol Chem* 2008; **283**: 32831–32838.
39 Cash JN, Angerman EB, Keutmann HT, Thompson TB. Characterization of follistatin-type domains and their contribution to myostatin and activin A antagonism. *Mol Endocrinol* 2012; **26**: 1167–1178.
40 Kootstra NA, Matsumura R, Verma IM. Efficient production of human FVIII in hemophilic mice using lentiviral vectors. *Mol Ther* 2003; **7**: 623–631.
41 Xiao X, Li J, Samulski RJ. Production of high-titer recombinant adeno-associated virus vectors in the absence of helper adenovirus. *J Virol* 1998; **72**: 2224–2232.
42 Qiao C, Li J, Zhu T, Draviam R, Watkins S, Ye X *et al.* Amelioration of laminin-alpha2-deficient congenital muscular dystrophy by somatic gene transfer of miniagrin. *Proc Natl Acad Sci USA* 2005; **102**: 11999–12004.
43 Wang B, Li J, Xiao X. Adeno-associated virus vector carrying human minidystrophin genes effectively ameliorates muscular dystrophy in mdx mouse model. *Proc Natl Acad Sci USA* 2000; **97**: 13714–13719.
44 Qiao C, Wang B, Zhu X, Li J, Xiao X. A novel gene expression control system and its use in stable, high-titer 293 cell-based adeno-associated virus packaging cell lines. *J Virol* 2002; **76**: 13015–13027.
45 Attisano L, Carcamo J, Ventura F, Weis FM, Massugué J, Wrana JL. Identification of human activin and TGF beta type I receptors that form heteromeric kinase complexes with type II receptors. *Cell* 1993; **75**: 671–680.
46 Inagaki K, Fuess S, Storm TA, Gibson GA, McTiernan CF, Kay MA *et al.* Robust systemic transduction with AAV9 vectors in mice: efficient global cardiac gene transfer superior to that of AAV8. *Mol Ther* 2006; **14**: 45–53.
47 Yang L, Jiang J, Drouin LM, Agbandje-McKenna M, Chen C, Qiao C *et al.* A myocardium tropic adeno-associated virus (AAV) evolved by DNA shuffling and in vivo selection. *Proc Natl Acad Sci USA* 2009; **106**: 3946–3951.
48 Smith RC, Lin BK. Myostatin inhibitors as therapies for muscle wasting associated with cancer and other disorders. *Curr Opin Support Palliat Care* 2013; **7**: 352–360.
49 Glass DJ. Skeletal muscle hypertrophy and atrophy signaling pathways. *Int J Biochem Cell Biol* 2005; **37**: 1974–1984.
50 Wrana JL, Attisano L, Carcamo J, Zentella A, Doody J, Laiho M *et al.* TGF beta signals through a heteromeric protein kinase receptor complex. *Cell* 1992; **71**: 1003–1014.
51 Liu N, Jiao T, Huang Y, Liu W, Li Z, Ye X. Hepatitis B virus regulates apoptosis and tumorigenesis through the microRNA-15a-Smad7-transforming growth factor beta pathway. *J Virol* 2015; **89**: 2739–2749.
52 Song X, Thalacker FW, Nilsen-Hamilton M. Synergistic and multidimensional regulation of plasminogen activator inhibitor type 1 expression by transforming growth factor type beta and epidermal growth factor. *J Biol Chem* 2012; **287**: 12520–12528.
53 Gardner S, Alzhanov D, Knollman P, Kuninger D, Rotwein P. TGF-beta inhibits muscle differentiation by blocking autocrine signaling pathways initiated by IGF-II. *Mol Endocrinol* 2011; **25**: 128–137.
54 Park I, Son HK, Che ZM, Kim J. A novel gain-of-function mutation of TGF-beta receptor II promotes cancer progression via delayed receptor internalization in oral squamous cell carcinoma. *Cancer Lett* 2012; **315**: 161–169.
55 Ramirez AM, Wongtrakool C, Welch T, Steinmeyer A, Zugel U, Roman J. Vitamin D inhibition of pro-fibrotic effects of transforming growth factor beta1 in lung fibroblasts and epithelial cells. *J Steroid Biochem Mol Biol* 2010; **118**: 142–150.
56 Gangopadhyay SS. Systemic administration of follistatin288 increases muscle mass and reduces fat accumulation in mice. *Sci Rep* 2013; **3**: 2441.
57 Abe Y, Minegishi T, Leung PC. Activin receptor signaling. *Growth Factors* 2004; **22**: 105–110.
58 Canalis E, Economides AN, Gazzerro E. Bone morphogenetic proteins, their antagonists, and the skeleton. *Endocr Rev* 2003; **24**: 218–235.
59 Gumienny TL, Padgett RW. The other side of TGF-beta superfamily signal regulation: thinking outside the cell. *Trends Endocrinol Metab* 2002; **13**: 295–299.
60 Keutmann HT, Schneyer AL, Sidis Y. The role of follistatin domains in follistatin biological action. *Mol Endocrinol* 2004; **18**: 228–240.
61 Winbanks CE, Weeks KL, Thomson RE, Sepulveda PV, Beyer C, Qian H *et al.* Follistatin-mediated skeletal muscle hypertrophy is regulated by Smad3 and mTOR independently of myostatin. *J Cell Biol* 2012; **197**: 997–1008.
62 Harrington AE, Morris-Triggs SA, Ruotolo BT, Robinson CV, Ohnuma S, Hyvonen M. Structural basis for the inhibition of activin signalling by follistatin. *EMBO J* 2006; **25**: 1035–1045.
63 Tsuchida K, Arai KY, Kuramoto Y, Yamakawa N, Hasegawa Y, Sugino H. Identification and characterization of a novel follistatin-like protein as a binding protein for the TGF-beta family. *J Biol Chem* 2000; **275**: 40788–40796.
64 Zamani N, Brown CW. Emerging roles for the transforming growth factor-{beta} superfamily in regulating adiposity and energy expenditure. *Endocr Rev* 2011; **32**: 387–403.

Supplementary Information accompanies the paper on Experimental & Molecular Medicine website (http://www.nature.com/emm)